DOI: 10.21062/mft.2025.077 http://www.journalmt.com

Heat Treatment-Induced Microstructural Changes in Selectively Laser Melted AlSi10Mg Alloy

Alice Chlupová (0000-0002-4411-5585)*, Jakub Poloprudský (0000-0001-5109-587X), Michal Jambor (0000-0001-9786-2034), Jaromír Brůža (0009-0004-3176-3075), Ladislav Poczklán (0000-0002-4516-7635), Jiří Man (0000-0002-6196-1580)
Institute of Physics of Materials, The Czech Academy of Sciences, Žižkova 513/22, 616 00 Brno, Czech Republic, *E-mail: chlupova@ipm.cz

The study examines the effect of various post-processing heat treatments on the microstructural evolution and hardness of the AlSi10Mg alloy produced by selective laser melting (SLM). The alloy was examined in the as-built (AB) condition and after three heat treatment regimes: direct aging (DA, 160°C/5 h), stress relieving (SR, 300°C/2 h), and solution annealing followed by artificial aging (SA, 520°C/2 h + 170°C/4 h) to better understand the solidification and consolidation processes. A multiscale characterization using OM, SEM, EBSD, TEM, and EDS was performed to reveal the changes in specific microstructures due to additive manufacturing and different levels of heat treatment. The AB state exhibited a fine cellular network of Si within an α-Al matrix, and high hardness (approx. 138 HV1). The DA treatment preserved cellular morphology with mild coarsening, whereas SR led to partial fragmentation of the Si network and a significant drop in hardness (approx. 83 HV1). The SA condition caused recrystallization, Si spheroidization, and formation of Mg- and Fe-rich precipitates, accompanied by moderate hardness recovery (approx. 104 HV1). The persistent crystallographic texture was confirmed across all states.

Keywords: Selective Laser Melting, Heat Treatment, AlSi10Mg, Microstructure, Properties

1 Introduction

Selective laser melting (SLM) is a method of additive manufacturing based on localized melting of metallic powder layer-by-layer using a laser as a high-power-density heat source. The parameters of SLM, such as laser power, scanning speed, hatching distance, and layer thickness, can be optimized and tailored to achieve specific microstructures with minimal porosity and corresponding mechanical properties. Materials used in additive manufacturing are usually popular structural materials. In addition to the basic mechanical characteristics, such as strength and ductility, they must also exhibit low reflectivity and high weldability, which are imperative for the SLM process. AlSi10Mg alloy is reasonably easy to process by SLM [1,2] due to its silicon content being close to the eutectic composition, which provides good pourability [3]. This lightweight material, which is harder and stronger than pure aluminum due to the formation of Mg_2Si precipitates, is widely used mainly in the aerospace and automotive industries [4]. Generally, all materials prepared by SLM exhibit a typical hierarchical structure created by melt pools and cells of high-density dislocation walls arranged into a honeycomb pattern. The presence of a certain amount of very fine oxide inclusions at cell boundaries can be expected. It all provides highly increased strength, nevertheless, at the expense of ductility [3]. The epitaxial grain growth through melting pools in the building direction (BD) leads to the development of texture, resulting in mechanical anisotropy [5]. Moreover, high cooling rates, together with repeated heating/cooling cycles inherent to the SLM process, produce material with strongly nonequilibrium microstructures that may exhibit high internal stresses [6,7,8]. It is advisable to perform an appropriate post-process heat treatment on additively manufactured materials. There are various heat treatment procedures, ranging from mild conditions to relieve internal stress, up to a substantial microstructure modification and full recrystallization [9]. Heat treatment of SLMed parts typically follows procedures developed for conventionally manufactured materials, with little to no special attention given to the distinct microstructure introduced by the SLM process [10]. Since even small changes within the microstructure may strongly impact the material response to external loading, the effect of heat treatment on the microstructure of materials prepared by SLM must be studied thoroughly, especially in the case of materials, such as AlSi10Mg, which exhibit precipitation strengthening/hardening. Moreover, the oxide particles (primarily Al_2O_3) are almost always present in AlSi10Mg prepared by the SLM technique, where their presence arises either from the surface layer on the gas-atomized powder particles or from the residual oxygen in the chamber [11]. The effect of these oxides

can be both beneficial and detrimental, depending on their size and distribution. They may offer modest dispersion-strengthening when finely distributed; nevertheless, they can reduce fatigue life if they are coarse. Their extent depends strongly on SLM process parameters, as well as on the conditions of heat treatment, as they may coarsen. This work focuses on tailoring the heat treatment procedures to reach a modified microstructure of AlSi10Mg, produced by additive manufacturing using SLM. Since the microstructure, strength, and plasticity are closely related, it is necessary to thoroughly tune the heat treatment of materials produced by SLM. Heat treatment at a lower temperature (170 °C) facilitates phase transformations and maximizes the material's hardness. It is also recommended to overcome the anisotropy of hardness due to different printing directions. Nevertheless, in the case of engine parts, long-term microstructural stability must be considered, and therefore, particular attention should be paid to the effect of long-term exposure to only slightly elevated temperatures. The heat treatment at medium temperatures is related to stress relief, while high-temperature treatment, such as solution annealing, provides dissolution of alloying elements for further precipitation hardening. To evaluate the microstructural changes caused by three selected types of heat treatment, various microscopic techniques and analyses were employed (OM, SEM, TEM, EBSD). Hardness measurement was performed to assess the effect of mechanical properties on heat treatment conditions.

2 Materials and methods

2.1 Material and SLM processing conditions

Gas-atomized AlSi10Mg powder with a particle size range of 15–45 μm was used for the SLM production of samples. The chemical composition is listed in Table 1. The SEM micrograph of powder morphology and internal crystallographic structure of particles, as revealed using an EBSD map in IPF colouring, is shown in Fig. 1. The powder consists of particles exhibiting predominantly spherical morphology with smooth surfaces, along with the presence of smaller satellite particles attached to the main spheres.

The samples from experimental material were manufactured at the VŠB-TUO in Ostrava using SLM as an additive manufacturing method. They were fabricated using a chessboard print strategy, in small blocks with dimensions of 10x10x20 mm. A Renishaw AM 400 additive manufacturing system, equipped with a 400 W laser and a 70 μm focal diameter, operated under a protective argon atmosphere. Processing parameters are as follows: a layer thickness of 30 μm, a hatch distance of 40 μm, a laser power of 350 W, and a scanning speed of 1150 mm/s. Platform preheating was not adopted.

Tab. 1 *The chemical composition of AlSi10Mg alloy powder (wt.%)*

Al	Si	Mg	Fe	Mn	Ti	Cu	Zn
Bal.	9-11	0.25-0.45	0.55	0.45	0.15	0.05	0.1

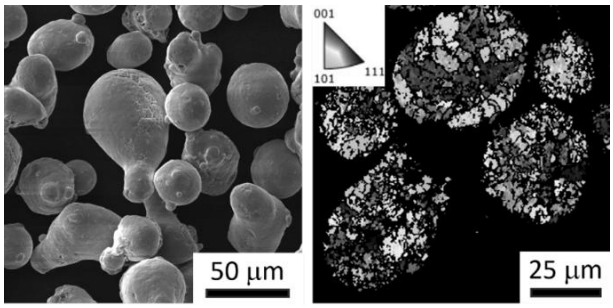

Fig. 1 *SEM micrograph and EBSD crystallographic analysis of AlSi10Mg powder*

2.2 Heat treatment

Heat treatment of the SLMed variant of the AlSi10Mg alloy is based on conventional procedures. Heat treatments assigned as T5 or T6 are the most frequent options. T5 is artificial aging, considered a low-temperature treatment, and T6 is solution annealing followed by water quenching and aging. Alloying with magnesium can refine the eutectic Si phase in AlSi10Mg alloy and promote the formation of Mg2Si precipitates when subjected to age-hardening heat treatments. Typical heat treatments for Al alloys are as follows:

- Annealing (between 300 and 410°C) is essentially employed to recrystallize the deformed structure after cold working of conventionally produced materials. In the case of additively manufactured parts, it also relieves the internal stresses [9]. The typical process for eliminating residual stress introduced by 3D printing involves artificial aging at a temperature of 300 °C [7]. It provides a maximum ductility and minimum hardness [12], [13]. The level of stress relief increases with growing temperature, but under certain conditions, it may result in a considerable drop in material strength due to rupture of the Si network.

For SLMed parts being stress-relieved, it is therefore essential to preserve the virgin Si network as much as possible.

- Homogenization (typically between 480 and 540°C) is usually performed in the as-cast condition, to redistribute the alloying elements for the precipitation of particles [9]. This is usually not the final heat treatment; subsequent processing regimes are applied thereafter.
- Solution annealing is conducted to dissolve the maximum hardening elements into the solid solution, homogenize the composition, and spheroidize the Si phase. Following quenching retains the dissolved phase and suppresses the precipitation [14].
- Aging aims to obtain a uniform distribution of precipitates that strengthens the alloys. Natural aging is conducted at room temperature, whereas artificial aging is performed at elevated temperatures with relatively long soaking times. Optimisation of heat treatment conditions, especially temperature and time range, is crucial to prevent under-aging (UA) or over-aging (OA). Nevertheless, they are not always undesirable; UA and OA are frequently employed to enhance stability or corrosion resistance, and the improvement of fatigue performance [15]. Direct aging (DA) balances the mechanical properties and the stress removal [16]. It promotes the precipitation of nano-scaled Si phases and preserves a network-like Si structure. Therefore, the strength of the peak-aged alloy increases while the ductility decreases.

A thorough literature survey was conducted to select the three most useful procedures for the heat treatment of our samples. To analyze the effect of the chosen heat treatment on the evolution of microstructure, a thorough microstructural study was performed after selected types of heat treatment, denoted as DA, SR, and SA (see detailed description in Table 2), and the results obtained were compared to those for the AB state.

Tab. 2 *Variable material states of AlSi10Mg alloy and parameters of heat treatment (HT)*

AB (as-built)	**DA** (direct aging)	**SR** (stress relieving)	**SA** (solution annealing + artificial aging)
without HT	160°C/5h/AC (T5)	300°C/2h/AC	520°C/2h/WQ + 170°C/4h/AC (T6)
AC = air cooling, WQ = water quenching			

2.3 Metallographic preparation

The morphology of the powder for SLM manufacturing was observed after the powder was mounted on carbon tape. EBSD observation of powder and its internal crystallographic structure and orientation required mounting it in resin, polishing it with standard metallographic practices, followed by polishing using colloidal silica (10 min, OPS), and finally polishing using VibroMet 2 Vibratory Polisher Buehler.

The SLMed samples were studied in the AB state, and after several heat treatment procedures (DA, SR, SA). The microstructural changes were typically observed in both directions relative to the BD, i.e., in the top view (surface perpendicular to the BD) and the side view (surface parallel to the BD). Samples for microstructure examinations were embedded in resin, and a 10 x 10 mm area was polished following standard metallographic practices. Chemical etching was applied to reveal structural phases and morphological features, such as melt pool lines and cellular dislocation substructure, by immersion into Keller's etchant for 10 seconds [13]. For EBSD, the following procedure was adopted: mechanical grinding and polishing, followed by colloidal silica polishing (5 min, OPS), and finally polishing using a VibroMet 2 Vibratory Polisher (Buehler).

2.4 Microstructure observation and porosity characterisation

The microstructure was examined in two principal sections with respect to the BD, namely parallel and perpendicular to BD. Initial microstructural observation was performed using an Olympus DSX1000 digital optical microscope (OM, Tokyo, Japan).

Detailed microstructural analysis was conducted using a Tescan LYRA 3 XMU FEG/SEMxFIB scanning electron microscope (SEM, Tescan, Czech Republic). The SEM is equipped with an EBSD Symmetry and EDS Ultimmax detectors, and Aztec software (Oxford Instruments, United Kingdom).

A Talos F200i transmission electron microscope (TEM, Thermo Fisher Scientific, Czech Republic) operating at 200 kV was used to investigate the internal dislocation arrangement and phase distribution in the examined materials. The microstructures were examined using bright-field (BF) imaging in scanning transmission electron microscopy (STEM) mode and chemical element distribution mapping using energy-dispersive spectroscopy (EDS). Specimens for TEM

were mechanically thinned using sandpapers and diamond suspensions, followed by ion milling using the Gatan precision ion polisher PIPS II.

For the porosity evaluation, i.e., density determination of additively manufactured samples, Archimedes' principle was adopted [17]. This approach is considered more accurate than image analysis because it takes into account the entire volume. The weight of the samples was measured on air and in acetone. As the ideal density for AlSi10Mg alloy, a value of 2660 kg/m³ was used, allowing the relative density of samples prepared by SLM and heat-treated to be calculated.

2.5 Hardness measurement

A DuraScan 70 G5 ZwickRoell hardness tester was used to measure HV1 values (with the loading force of 9,807 N). Hardness was measured in the plane parallel to the BD, i.e., on the side surface. A standard Vickers indenter was used for the measurement. 5 measurements were evaluated on a polished surface (final preparation was carried out mechanically and completed with a 1μm diamond suspension to produce a mirror-like finish).

3 Results and discussion

The SLM process typically provides a complex hierarchical microstructure. To analyze the microstructural evolution of AlSi10Mg alloy prepared by the SLM method and exposed to three types of heat treatment procedures, several techniques were adopted, including optical microscopy (OM), electron microscopy (SEM, TEM), and EBSD analysis. Every observation technique provides the results of microstructure evolution studies at different magnifications and from various points of view.

Results of OM observation in a dark field view at relatively small magnification in a plane perpendicular or parallel to build direction for all material states are shown in Fig. 2. AB state, as well as DA and SR state (Fig. 2a, b, c) provided a nice view of the microstructure with melt pool pattern, which is typical for the additively manufactured structures due to the localized melting and rapid solidification. The SA state exhibits recrystallization, so the melt pool pattern in both directions disappeared (Fig. 2d).

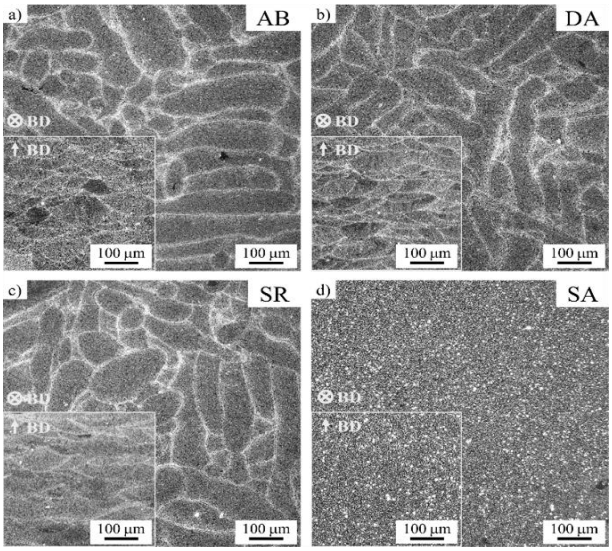

Fig. 2 *Microstructure of the AlSi10Mg alloy manufactured by SLM and heat-treated (OM, dark field)*

The typical but unwanted feature of additively manufactured materials is porosity, as it is a weakening factor for the mechanical properties of primary importance. Our samples contained a certain number of pores; most of them exhibited a spherical shape typical of entrapped gas pores, and these pores were distributed randomly within the individual melt pools. Sometimes the pores are localized preferentially between melt pools corresponding to two successive layers; nevertheless, in our case, the pores were distributed randomly inside the individual melt pools. The values of density, relative density, and porosity in % are calculated and listed in Table 3. The material in the AB state exhibits a satisfactory value of relative density, while any heat treatment causes a slight increase in the porosity. The highest porosity was observed in the SA state. This can be attributed to material recrystallization, the coarsening of precipitates, and possibly the coagulation of trapped gas bubbles, as well as changes in density resulting from phase transformation following solution annealing and precipitation.

Tab. 3 *Results of density and porosity measurements for SLM AlSi10Mg alloy in various material states*

Material state	Density [kg/m³]	Relative density [%]	Porozity [%]
AB	2655.2 ± 0.3	99.82	0.18 ± 0.01
DA	2635.8 ± 0.9	99.09	0.91 ± 0.03
SR	2643.9 ± 0.6	99.39	0.61 ± 0.02
SA	2601.7 ± 0.9	97.81	2.19 ± 0.03

SEM analysis of the microstructure was performed to observe the hierarchical microstructure introduced by SLM and modified by heat treatment in more detail. Contrary to OM, which is favorable for melt pool identification and porosity evaluation, SEM provides a higher magnification study, focused on the cellular morphology of the Si network with respect to the melt pool boundary (MPB). The size of the cells depends on the position within the melt pool, where the boundary cells exhibit slightly higher diameters than the

inner cells. The typical diameter of the cellular substructure, as evaluated using SEM micrographs, is approximately 600–800 nm. The stability of cellular structure upon exposure to heat treatment plays a significant role in the resulting mechanical properties. More detailed information about grain/cell size is provided later in the chapter focused on EBSD results.

Since heat treatment was at the centre of attention of the present study, the microstructures achieved by heat treatments were compared to the AB state, i.e., with the microstructure obtained directly after SLM. Fig. 3 shows SEM micrographs. In Fig. 3a1, b1, c1, d1, there is an overview of the microstructure at small magnification. It seems, at this magnification level, that the first three material states have similar microstructure, i.e., no serious changes between AB state and heat-treated DA and SR states were observed, which agrees with the OM observation presented in Fig. 2. The only difference can be recognized for the SR state, where the melt pool boundaries partially dissolved. The SA state exhibited a significant change in microstructure, characterized by dissolved melt pool boundaries and the precipitation of Si particles. The higher magnification pictures of the microstructure (see Fig. 3a2, b2, c2, d2) depict the morphology of the fine- and coarse-grained parts within an individual melt pool, while coarser cells with a Si network are concentrated along the MPB. Similar results were observed in the work of Měsíček for the artificial aging at 170°C [7]. The heat treatment leading to a similar microstructure as in our SR state was studied in [18], where the treatment temperatures and durations were adjusted by calorimetric results to achieve the desired properties. While direct T6-style studies on AlSi10Mg in SLM are rather limited [4] procedures developed for conventional Al-Mg-Si alloys are usually adopted. In our case, the heat treatment labelled SA combines the solution annealing with artificial aging. It leads to the transition of eutectic Si from a fine interconnected network to bigger and discrete Mg_2Si precipitates.

The detailed micrographs of the microstructure are depicted in Fig. 4. The darker interiors (core of cells) in Fig. 4a correspond to the α-Al matrix, while the bright phase creating a continuous network around it is the Si phase, in some places forming areas of eutectic islands of Si. After heat treatment at low temperature (the DA state), the Si network around Al cells is still present; nevertheless, it is coarsened (see Fig. 4b). Further increase in treatment temperature (the SR state) caused the rupture of the Si network and precipitation of fine Si particles (see Fig. 4c). Very high temperature of solution annealing leads to globular or blocky morphology of Si particles (see Fig. 4d). The presence of Fe-containing intermetallic phase Al5SiFe-β with rod shape morphology or needle-like shape [19], was also observed in the case of the SA state; nevertheless, on the SEM pictures (Figs. 3 and 4), it is presented by holes, because the Kroll´s reagent etched them.

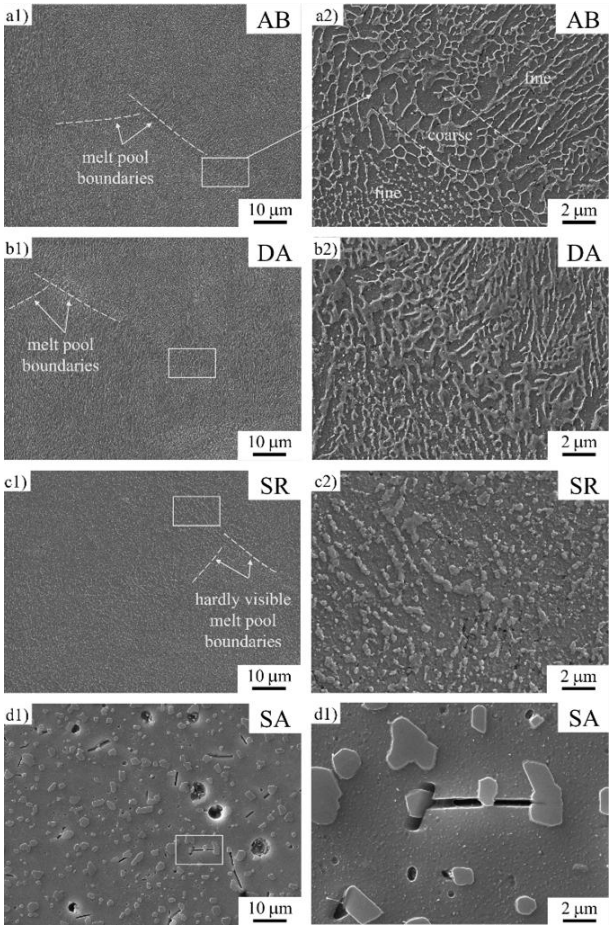

Fig. 3 *Microstructure of the AlSi10Mg alloy manufactured by SLM in as-built and heat-treated states (Left – overview with either melt pool pattern or partially and fully recrystallized microstructure; right – higher magnification picture with either cellular structure of Si network or Si precipitates (SEM))*

The heat treatment must be carefully tuned. If performed properly, it can provide decreased hardness as a trade-off for increased ductility. According to the work of Li [14] the plastic elongation of the SA state vs. the AB state is approximately 3 times higher, because this kind of heat treatment overrides the precipitation strengthening obtained in the DA or SR state. The SA state also shows an increase in fatigue life up to 5 times [14]. The formation of globular Si particles typical for the SA state reduces stress concentrations and delays void nucleation, i.e., it can be beneficial for enhancing fracture toughness [20]. The T6-based heat treatment (the SA state) of the SLMed variant of AlSi10Mg alloy shows approximately 35% better wear resistance due to larger and fewer Si precipitates [21].

EBSD maps in IPF coloring, with band contrast and enhancement of grain boundaries, are presented in Fig. 5 a1, b1, c1, d1. Band contrast highlights

significant fractions of low-angle boundaries within cells, i.e., exhibiting misorientation lower than 5°. This finding aligns with those of Yan [22]. EBSD analysis reveals the effect of heat treatment on grain morphology, the orientation and size of columnar grains, as well as the evolution/disintegration of cellular structure depending on temperature exposure during the heat treatment. All material states exhibit texture (see Fig. 5 a2, b2, c2, d2), i.e., the directed orientation of the grains due to epitaxial grain growth through melt pools. The MPB is indicated by yellow dashed lines, as shown in the SEM picture (see Fig. 3a2). Elongated grains grow independently on the MPB and usually keep the BD. Even in the SA state, with the highest temperature of heat treatment, where the MPB disappeared, and precipitation of big Si particles occurred, the texture/preferred orientation prevailed. Texture is manifested by the value of Multiple Uniform Distribution (MUD), which reached the value of approximately 3, and the preferred orientation of grains is in the [001] direction, similar to the results in [19] and [22]. The strongest texture, nevertheless, is in the case of the AB state.

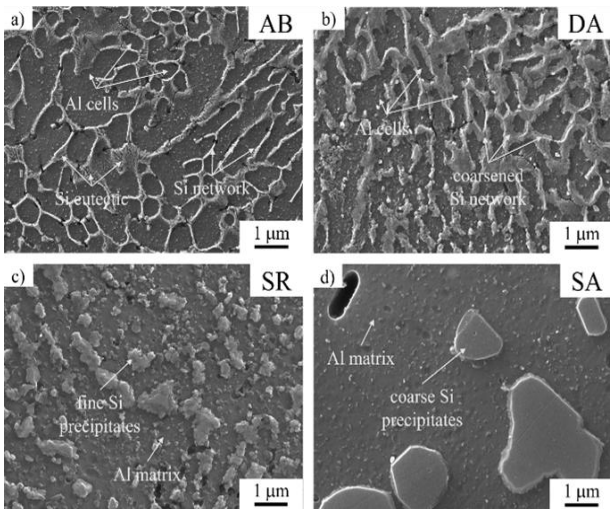

Fig. 4 *High magnification SEM images of the cellular pattern of Si network or Si precipitates in AlSi10Mg alloy prepared by SLM in the as-build and heat-treated states*

In dark-field imaging of TEM, the cell boundaries exhibit a typical bright contrast, indicating an enrichment of heavier elements. The bright-field imaging (BF) in scanning transmission electron microscopy (STEM) is used to gain a general contrast and overall view of morphology and grain structure. BF micrographs for all material states under investigation are presented in Fig. 6. The results for the AB state are shown in Fig. 6a as an overview, and the details of the internal structure of the typical cellular (honeycomb) structure. Fig. 6b and Fig. 6c show the partial dissolution of cellular structure in DA and SR states; nevertheless, it is still possible to observe them. Finally, Fig. 6d exhibits the alloy in the SA state, i.e., after thermal treatment, resulting in the recrystallization and complete rearrangement of the Si network, along with a distinct dislocation pattern. In the left corner of Fig. 6d, a particle of the AlSiFe intermetallic phase, typical of a rod-shaped morphology, was captured.

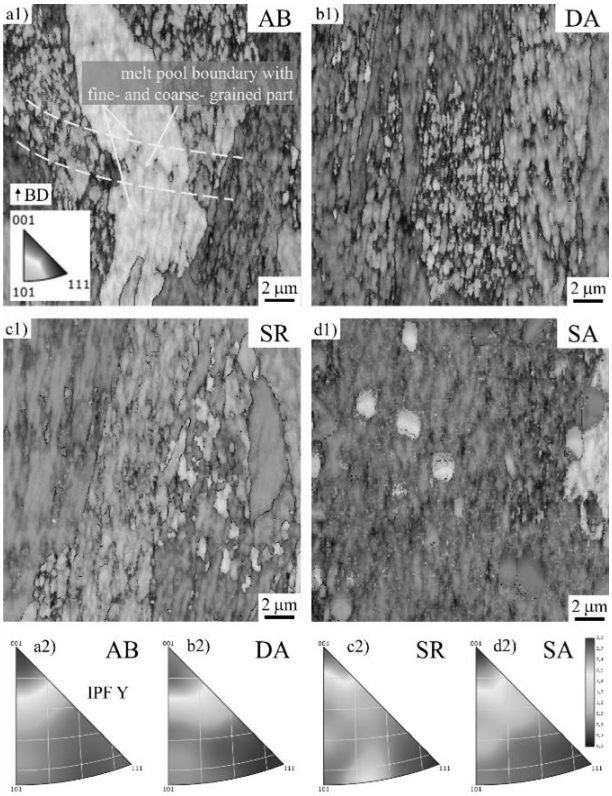

Fig. 5 *EBSD orientation maps in IPF coloring a1), b1), c1), d1) and corresponding IPF Y figures describing texture induced by SLM process a2), b2), c2), d2) as revealed for SLM AlSi10Mg alloy in as-built and heat-treated states*

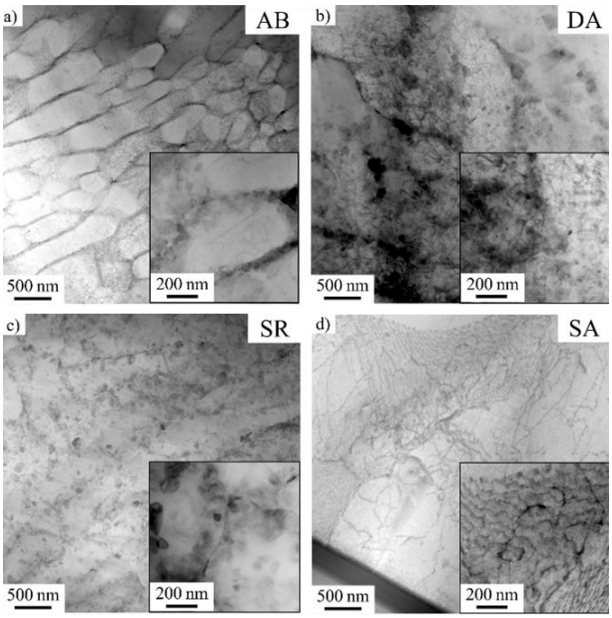

Fig. 6 *TEM micrographs of the AlSi10Mg alloy manufactured by SLM and heat-treated*

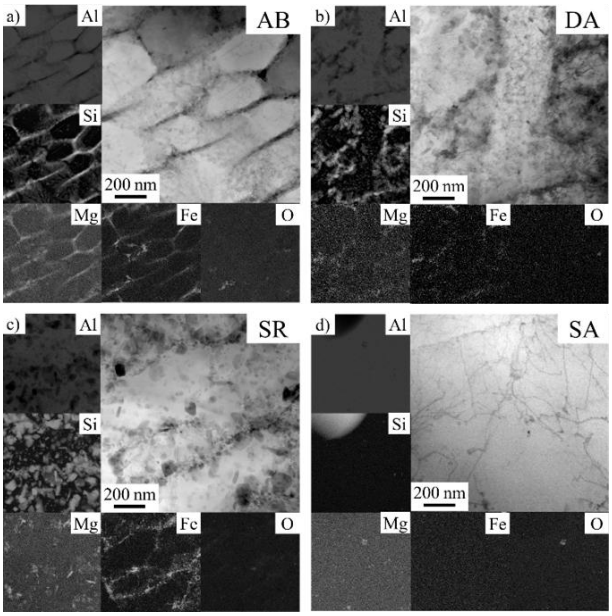

Fig. 7 *TEM micrographs and EDS maps with distribution of main elements on details with particles in the AlSi10Mg alloy manufactured by SLM and heat-treated*

Results of TEM/EDS analysis of all four material states are in Fig. 7. The high magnification BF images are accompanied by elemental maps, showing nicely the distribution of alloying elements and arrangement of Si into the network within cell walls (see Fig.7a for the AB state). The presence of fine oxide particles, as described in [11], located usually at cell boundaries, was not observed, neither in the case of the state that was heat-treated at the highest temperature (SA), when their coarsening could be expected. Assuming that these oxide particles are very fine, observation using TEM appears to be the most suitable for their identification. Unfortunately, this method also has its disadvantages, as it is demanding, time-consuming, and very localized. Therefore, it provides rather a qualitative assessment of the presence, size, and location of particles than an exact determination of their quantity in the volume of the material. The situation with the presence of Mg_2Si precipitates is quite similar. According to the work [12] they are related to the age hardening. In the case of the DA state (see Fig. 7b), the temperature of heat treatment was gentle enough not to dissolute the Si network and only led to the coarsening of it (as confirmed by SEM in Fig. 4b). The SR state (see Fig. 7c) shows dissolution of the Si network; only the elemental map for Fe shows the last hints of cellular morphology. The SA state with the highest temperature results in the formation of Fe-rich needle-like precipitates (not captured in Fig. 7d), blocky precipitates of Si (see the elemental map in Fig. 7d), but the most important is the precipitation of fine Mg precipitates, which are crucial for age hardening.

3.1 Hardness

The as-built state of the SLMed materials generally exhibits a higher hardness than its conventional counterpart, which is attributed to:

- 1) Smaller grain/cell size (grain boundary strengthening, similarly as in Hall-Petch relationship),
- 2) Fine cellular structure with high dislocation density at cell boundaries (dislocation strengthening),
- 3) Numerous nano-scaled oxide inclusions (Orowan strengthening by oxides).

In our experiment, the situation is slightly different because this alloy can undergo aging, which increases the hardness of the material, while certain kinds of post-SLM heat treatment (stress reliving) result in a decrease in microhardness [9]. Hardness measurements using the Vickers technique were performed on all our samples on a plane parallel to the BD. The results are listed in Table 4. Due to a strong anisotropy of mechanical properties, it is necessary to note that the hardness measurement for the other orientation, i.e., perpendicular to BD, can show slightly different values.

Tab. 4 *Hardness values of AlSi10Mg alloy prepared by SLM in four material states*

State	**AB** (without HT)	**DA** (160°C/5h/AC)	**SR** (300°C/2h/AC)	**SA** (520°C/2h/WQ + 170°C/4h/AC)
Hardness	138.4 ± 5.7 HV1	140.0 ± 1.6 HV1	83.5 ± 3.5 HV1	103.8 ± 1.1 HV1
Result	fine microstructure due to rapid melting and solidification, high internal stress	suitable for improving strength, without solution annealing	removal of residual stress, coagulation of Si precipitates, reduction of hardness, increase of ductility	precipitation of fine particles, increased strength and hardness

4 Conclusions

In this study, the aluminum alloy AlSi10Mg fabricated by SLM was systematically investigated regarding its microstructure and hardness evolution in the as-build state (AB) and after three distinct post-processing heat treatments: direct aging (DA, 160 °C / 5 h), stress relieving (SR, 300 °C / 2 h), and solution annealing followed by artificial aging (SA, 520 °C / 2 h

+ 170 °C / 4 h). A comprehensive multiscale characterization approach employing OM, SEM, EBSD, TEM, and EDS was applied to elucidate the structural changes induced by thermal exposures of various intensities.

The AB condition was characterized by a fine hierarchical cellular structure with a strong columnar grain orientation along the BD, high dislocation density, and a network of eutectic silicon. This microstructure provided a high level of hardness, but it suffers from lower plasticity, considerable residual stress, and inherent anisotropy. The DA state preserved the general cellular morphology and silicon network while initiating mild coarsening. The SR state led to partial degradation of the silicon network, evidenced by its fragmentation and the appearance of isolated Si particles, although melt pool patterns remained partially visible. In contrast, the SA treatment resulted in significant recrystallization and depletion/disappearance of the melt pool structure. The Si network transformed into a structure with an aluminum matrix and coarse and fine Si precipitates.

EBSD analysis confirmed a [001] type crystallographic texture persistently present within the AlSi10Mg alloy prepared via SLM, irrespective of the adopted variant of post-heat treatment. The texture was evaluated in the direction parallel to BD. The strongest texture for the AB state, and a gradual decline in the LAGB (low-angle grain boundary) fraction with increasing temperature, was documented. The grain size slightly increased in the SA condition; nevertheless, no severe grain coarsening was observed across all conditions.

The density and porosity analysis demonstrated that all heat treatments slightly increased porosity compared to the AB state, with the SA state showing the highest porosity (approx. 2.19%), likely due to the coalescence of gas pores during prolonged high-temperature exposure and to density changes during phase transformation at precipitation.

Hardness measurements revealed a non-monotonic trend: both the AB and SA states displayed high hardness values (approx. 140 HV1), while the SR state exhibited the strongest decrease in hardness (approx. 83 HV1), consistent with partial stress relief and Si network disruption. The SA condition exhibited moderate hardness due to precipitation hardening (approx. 103 HV1), and according to the literature, it is expected to significantly enhance ductility and fatigue performance.

TEM and EDS investigations confirmed the evolution of dislocation structures and the presence and redistribution of the Si network into Si precipitates with heat treatment.

To summarize the results, the applied heat treatments enabled controlled tailoring of the microstructure and properties of SLMed AlSi10Mg alloy. The findings highlight the importance of optimizing thermal post-processing to strike a balance between strength, ductility, and long-term stability, particularly for high-performance applications such as aerospace and automotive components. Among the treatments studied, the T6-like SA condition represents the most promising procedure.

Funding/Acknowledgment

This study was financially supported by the Czech Science Foundation under project No. GA23-05372S. Ladislav Poczklán also acknowledges the support of the Czech Academy of Sciences under the framework of the Lumina quaeruntur project. The authors would like to thank VŠB-TUO in Ostrava for the 3D printing of experimental material.

References

[1] ŠUTKA, J., MEDVECKÁ, D., KOŇAR, R., BRUNA, M., MATEJKA, M. (2023). Evaluation of Selected Technological Parameters for Selective Laser Melting of AlSi10Mg Metal Powder. In: *Manufacturing Technology*, Vol. 23, No. 1, pp. 110–117.

[2] FOUSOVÁ, M., DVORSKÝ, D., VOJTECH, D. (2017). Additively Manufactured Aluminium AlSi10Mg Alloy. In: *Manufacturing Technology*, Vol. 17, No. 4, pp. 446–451.

[3] TREVISAN, F., CALIGNANO, F., LOZANO, J. A., et al. (2017). On the Selective Laser Melting (SLM) of the AlSi10Mg Alloy: Process, Microstructure, and Mechanical Properties. In: *Materials*, Vol. 10, No. 76, pp. 1–20.

[4] ABOULKHAIR, N. T., MASKERY, I., TUCK, C., ASHCROFT, I., EVERITT, N. M. (2016). The Microstructure and Mechanical Properties of Selectively Laser Melted AlSi10Mg: The Effect of a Conventional T6-like Heat Treatment. In: *Materials Science and Engineering A*, Vol. 667, pp. 139–146.

[5] YAP, C. Y., CHUA, C. K., DONG, Z. L., et al. (2015). Review of Selective Laser Melting: Materials and Applications. In: *Applied Physics Reviews*, Vol. 2, No. 041101, pp. 1–21.

[6] FANG, Z. C., WU, Z. L., HUANG, C. G., WU, C. W. (2020). Review on Residual Stress in Selective Laser Melting Additive Manufacturing of Alloy Parts. In: *Optics & Laser Technology*, Vol. 129, pp. 106283.

[7] MĚSÍČEK, J., DVORSKÝ, D., ČAPEK, J., et al. (2022). Effect of Artificial Aging on the Strength, Hardness, and Residual Stress of SLM

AlSi10Mg Parts Prepared from Recycled Powder. In: *Materials Science and Engineering A*, Vol. 855, pp. 143900.

[8] BARTOŠÁK, M., MURANOVA, L., KOUTNÝ, D., et al. (2025). Low-Cycle Fatigue of Laser Powder Bed Fusion-Processed AlSi10Mg Using Recycled Powder: Experiments and Machine-Learning-Assisted Lifetime Prediction. In: *Materials & Design*, Vol. 253, pp. 113926.

[9] LALEH, M., ZHANG, X., YUAN, L., et al. (2023). Heat Treatment for Metal Additive Manufacturing. In: *Progress in Materials Science*, Vol. 134, pp. 101051.

[10] ISHFAQ, K., ABDULLAH, M., MAHMOOD, M. A. (2021). A State-of-the-Art Direct Metal Laser Sintering of Ti6Al4V and AlSi10Mg Alloys: Surface Roughness, Tensile Strength, Fatigue Strength and Microstructure. In: *Optics & Laser Technology*, Vol. 141, pp. 107366.

[11] TANG, M., PISTORIUS, P. C. (2017). Oxides, Porosity and Fatigue Performance of AlSi10Mg Parts Produced by Selective Laser Melting. In: *International Journal of Fatigue*, Vol. 94, pp. 192–201.

[12] ZHOU, L., MEHTA, A., SCHULZ, E., et al. (2018). Microstructure, Precipitates and Hardness of Selectively Laser Melted AlSi10Mg Alloy Before and After Heat Treatment. In: *Materials Characterization*, Vol. 143, pp. 34–44.

[13] ABOULKHAIR, N. T., TUCK, C., ASHCROFT, I., MASKERY, I., EVERITT, N. M. (2015). On the Precipitation Hardening of Selective Laser Melted AlSi10Mg. In: *Metallurgical and Materials Transactions A*, Vol. 46, No. 8, pp. 3337–3341.

[14] LI, W., LI, S., LIU, J., et al. (2016). Effect of Heat Treatment on AlSi10Mg Alloy Fabricated by Selective Laser Melting: Microstructure Evolution, Mechanical Properties and Fracture Mechanism. In: *Materials Science and Engineering A*, Vol. 663, pp. 116–125.

[15] LIU, Y., PAN, Q., LIU, B., YU, Q., LI, G., PAN, D. (2022). Effect of Aging Treatments on Fatigue Properties of 6005A Aluminum Alloy Containing Sc. In: *International Journal of Fatigue*, Vol. 163, pp. 107103.

[16] TANG, H., LI, W., WANG, X., et al. (2023). Effects of Direct Aging Treatment on Microstructure, Mechanical Properties and Residual Stress of Selective Laser Melted AlSi10Mg Alloy. In: *Journal of Materials Science & Technology*, Vol. 139, pp. 1–14.

[17] SPIERINGS, A. B., SCHNEIDER, M., EGGENBERGER, R. (2011). Comparison of Density Measurement Techniques for Additive Manufactured Metallic Parts. In: *Rapid Prototyping Journal*, Vol. 17, No. 5, pp. 380–386.

[18] FIOCCHI, J., BIFFI, C. A., COLOMBO, C., VERGANI, L. M., TUISSI, A. (2020). Ad Hoc Heat Treatments for Selective Laser Melted AlSi10Mg Alloy Aimed at Stress-Relieving and Enhancing Mechanical Performances. In: *JOM*, Vol. 72, No. 3, pp. 1130–1140.

[19] LEHNER, P., KOEPKE, J., SCHULZ, F., et al. (2024). Influence of the As-Built Surface and a T6 Heat Treatment on the Fatigue Behavior of Additively Manufactured AlSi10Mg. In: *International Journal of Fatigue*, Vol. 187, pp. 108479.

[20] WANG, L. F., LIU, S., JIANG, J., et al. (2018). Enhancement in Mechanical Properties of Selectively Laser-Melted AlSi10Mg Aluminum Alloys by T6-like Heat Treatment. In: *Materials Science and Engineering A*, Vol. 734, pp. 93–104.

[21] PARK, T. H., BAEK, M. S., SOHN, Y., LEE, K. A. (2020). Effect of Post-Heat Treatment on the Wear Properties of AlSi10Mg Alloy Manufactured by Selective Laser Melting. In: *Archives of Metallurgy and Materials*, Vol. 65, No. 3, pp. 1021–1028.

[22] YAN, X., ZHANG, Y., HUANG, L., et al. (2022). Modeling and Simulation Investigations on Microstructure Evolution During Additive Manufacturing of AlSi10Mg Alloy. In: *Metals*, Vol. 12, No. 10, pp. 1711.